Adaptive Sliding Mode Fault Tolerant Control for Autonomous Vehicle With Unknown Actuator Parameters and Saturated Tire Force Based on the Center of Percussion

Zhongchao Liang, Mingyu Shen, Jing Zhao, Zhongguo Li, *Member, IEEE*, Yongfu Wang, and Zhengtao Ding, *Senior Member, IEEE*

***Abstract*— With consideration of tire force saturation in vehicle motions, a novel path-following controller is developed for autonomous vehicles with unknown-bound disturbances and unknown actuator parameters. An adaptive sliding-mode fault-tolerant control (ASM-FTC) strategy is designed to stabilize the path-following errors without any information of disturbance boundaries, actuator fault boundaries and steering ratio from the steering wheel to the front wheels. By selecting the distance from the center of gravity to the center of percussion as the preview length, the effects of the lateral rear-tire force are decoupled and cancelled out, and then the preview error, which represents the path-following performance, can be only commanded by the front-tire force. To further address the issue of unknown tire-road friction limits, a modified ASM-FTC strategy is presented to improve the path-following performance as the lateral tire force is saturated. Simulation results show that the modified ASM-FTC controller demonstrates superior tracking performance over the normal ASM-FTC while the autonomous vehicle follows desired paths.**

***Index Terms*— Path following, autonomous vehicle, friction limits, tire force saturation, bound-unknown disturbances, unknown steering ratio.**

I. Introduction

MANY groups have begun to develop self-driving techniques for intelligent and autonomous vehicles over the past decade, and a significant number of profound, systematic and extensive research works have been reported [1]. Due to high traffic accident mortality and driving difficulty under some extreme conditions, it is of great significance and necessity to develop self-driving techniques for the increasing demands on safety motivations [2]. As a fundamental issue for autonomous vehicles, the path-following control strategy is devised to guarantee the offset errors between the autonomous vehicles and the desired paths (especially the lateral distance offset error) within reasonable and safe regions [3].

The principal mission of path-following control is to track desired paths, and to implement automatic steering operations for autonomous vehicles [4]. Many control schemes, such as proportional-integral-derivative (PID) control, model predictive control (MPC) and sliding-mode control (SMC), have been developed to construct path-following controllers. The traditional PID controllers are easy and effective [5], whereas are difficult to obtain high response performance while the system is complex and the states are constrained. To achieve optimal tracking performance, MPC algorithms are able to predict control variables for the next sampling time and guarantee the path-following accuracy, but searching for optimal solutions may increase the computational burdens [6], [7]. Among the various controller design methodologies, SMC method is an effective approach for nonlinear systems with uncertain disturbances, and has the simple variable structure with high control performance. The sliding-mode motion for the controlled system is independent of the matched external disturbances, and thereby holds strong robustness [8].

In order to deal with the nonlinear characteristics, parameter uncertainties and external disturbances [9], SMC has been widely used in the path-following system for autonomous vehicles [10]. With consideration of modeling errors and complex driving scenarios, the SMC algorithms are effective to improve the transient performance and follow the given paths [11]. However, since the discontinuous sign function is applied to reject the uncertainties, there always exists chattering phenomenon in the SMC controller [12]. To circumvent chattering, the saturation function is a simple choice to replace the discontinuous function. In addition, higher-order SMC strategy with nonlinear disturbance observer technique can be used to suppress chattering and achieve high tracking

Manuscript received 24 December 2020; revised 13 July 2021, 18 January 2022, 23 November 2022, and 23 February 2023; accepted 21 June 2023. This work was supported in part by the National Natural Science Foundation of China under Grant 51975109, in part by the Fundamental Research Funds for the Central Universities under Grant N2103018, and in part by the Joint Project of Natural Science Foundation of Liaoning Province of China under Grant 2021-KF-11-02. The Associate Editor for this article was B. Ayalew. *(Corresponding author: Jing Zhao.)*

Zhongchao Liang, Mingyu Shen, Jing Zhao, and Yongfu Wang are with the School of Mechanical Engineering and Automation, Northeastern University, Shenyang 110819, China, and also with the State Key Laboratory of Synthetical Automation for Process Industries, Northeastern University, Shenyang 110819, China (e-mail: liangzc@me.neu.edu.cn; shenmy@stumail.neu.edu.cn; zhaoj@mail.neu.edu.cn; yfwang@mail.neu.edu.cn).

Zhongguo Li is with the Department of Computer Science, University College London, WC1E 6BT London, U.K. (e-mail: zhongguo.li@ucl.ac.uk).

Zhengtao Ding is with the Department of Electrical and Electronic Engineering, The University of Manchester, M13 9PL Manchester, U.K. (e-mail: zhengtao.ding@manchester.ac.uk).

Digital Object Identifier 10.1109/TITS.2023.3289439

performance [13]. The conventional SMC algorithms always require the prior knowledge of the boundaries of uncertainties. Therefore, the adaptive sliding-mode control design techniques have been proposed to achieve the control objective in the presence of the parameter uncertainties [14].

Tire-road friction is the primary force in vehicle motions, and is physically limited by the adhesion coefficient of the tire-road surface and instantaneous normal tire load [15]. As the tire-road friction reaches its limit, the tire force constraints may result in system ineffective in certain situations [16], such as steering and braking. In order to address the issue of the tire force saturation, most existing articles mainly depend on the prior knowledge or the estimation of the tire-road friction limits. By using a predefined constraint for the steering input, the proposed saturation control strategy can effectively stabilize the path-following error and avoid reaching the tire-road friction limits [17], [18]. In terms of safety consideration, planning safety conditions while vehicle traversing given paths can be an alternative strategy to avoid exceeding the tire-road friction limits [19]. However, the boundary of the available tire force is required to know for the preset input constraint before the controllers have been implemented [20]. In addition, with the estimation algorithm of the tire force capacity, the braking or traction maneuver can be employed to adjust the direction of the resultant tire force while the tire force is saturated [21], [22], whereas the estimation algorithm always burdens the computing sources of the vehicle computing unit (VCU) [23]. Therefore, a more applicable solution is required to develop the path-following controller without the information of the tire-road friction limits.

In the path-following process, the lateral tire forces are commanded by the steering actuators, and the automatic operations can be calculated, as long as the accurate lateral tire force can be obtained. However, the nonlinear characteristics of the tire force may result in input faults, which in turn affect the designed path-following control system. Appropriate fault tolerant control (FTC) strategy can guarantee the reliability of the path-following control system in the autonomous vehicle [24], [25]. Therefore, FTC for the autonomous vehicle is of great importance to maintain acceptable path-following performance [26]. Resorting to the friction circle, the brake maneuver can minimize the lateral tire forces, and the high-level brake control algorithm combined with the existing yaw stabilizing controllers can be employed to prevent the rollover for the vehicles [27]. As the lateral and longitudinal tire forces increase beyond certain limits, the vehicle may exhibit performance degradation. Compared with the pure-slip controller, the controller using the combined-slip tire model can adjust the lateral tire forces and vary the longitudinal tire slip ratio to correct the oversteer responses of the vehicle [22]. By incorporating the combined-slip friction effects, the torque reconfiguring controller can effectively maintain the vehicle lateral motion within a stable region [23]. Even though the accurate tire model and the tire-road friction limit can facilitate the design of the control strategy, it is difficult to accurately measure or estimate all the parameters of the tire and road.

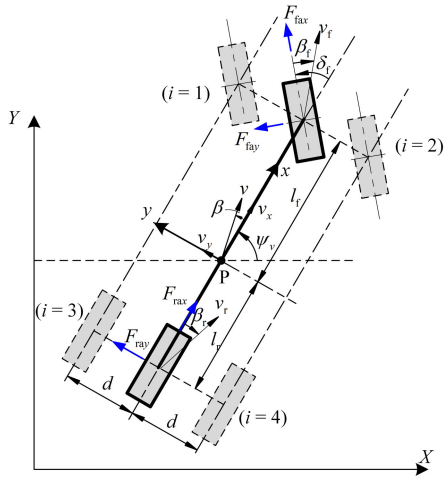

Fig. 1. Dynamic model for vehicle.

Motivated by the above discussions, in this paper, a robust controller is developed such that the vehicle can follow the given paths subject to unknown lateral tire force constraints and inaccurate models. The main contributions of this study are stated as follows.

1) By introducing the preview error as a path-following index, the distance from the center of gravity to the center of percussion is selected as the preview length. This is able to decouple and cancel the lateral force items of the rear tires in the path-following model, and facilitates the controller design in the analysis for the tire force saturation.
2) Without any information regarding the boundaries of uncertainties and disturbances, the boundaries of actuator faults and the steering ratio from the steering wheel to the front wheels, an adaptive sliding-mode fault-tolerant control (ASM-FTC) strategy is proposed to ensure the path-following accuracy for the autonomous vehicle.
3) On the basis of the center of percussion and the designed ASM-FTC strategy, a complement saturation control scheme is proposed to improve the path-following performance while the autonomous vehicle is driven under the extreme condition of saturated tire force with unknown tire-road friction limits.

The remainder of this paper is organized as the following. The vehicle dynamics and the problem formulation are established in Section II. The center of percussion and the controller design are presented in Section III. In Section IV, simulations are conducted to verify the proposed controllers. Finally, Section V presents the conclusion.

II. System Modelling and Problem Formulation

A. Vehicle Dynamic Model

1) Dynamic Analysis: The dynamics of a vehicle are shown in Fig. 1, and the subscript i represents the wheel ID. Meanwhile, the main parameters of the vehicle are described in Table I.

TABLE I
MAIN PARAMETERS FOR VEHICLE MODEL

Symbol	Value
m	Vehicle mass
I_Z	Yaw moment of inertia of vehicle
$l_\mathrm{f}/l_\mathrm{r}$	Distance from center of gravity (CG) to front/rear axle
d	Distance from CG to left/right wheel
R	Effective rolling radius of wheel
$F_{ix}/F_{iy}/F_{iz}$	Longitudinal/lateral/vertical force of wheel i
δ_f	Steering angle of front wheels
ψ_v/γ	Yaw angle/rate of vehicle
β/β_i	Sideslip angle of vehicle/wheel i
$v/v_x/v_y$	Total/longitudinal/lateral velocity of vehicle at CG
c_a	Aerodynamic drag term coefficient

The longitudinal motion along x-axis can be calculated by

$$m\left(\dot{v}_x - v_y\gamma + c_\mathrm{a}v_x^2\right) = F_{\mathrm{fa}x}\cos\delta_\mathrm{f} + F_{\mathrm{ra}x} - F_{\mathrm{fa}y}\sin\delta_\mathrm{f}, \quad (1)$$

where $F_{\mathrm{fa}x} = F_{1x} + F_{2x}$ and $F_{\mathrm{ra}x} = F_{3x} + F_{4x}$ are the total longitudinal forces of the front and rear tires, respectively; $F_{\mathrm{fa}y} = F_{1y} + F_{2y}$ is the total lateral force of the front tires.

The lateral motion along y-axis can be written as

$$m\left(\dot{v}_y + v_x\gamma\right) = F_{\mathrm{fa}x}\sin\delta_\mathrm{f} + F_{\mathrm{fa}y}\cos\delta_\mathrm{f} + F_{\mathrm{ra}y}, \quad (2)$$

where $F_{\mathrm{ra}y} = F_{3y} + F_{4y}$ is the total lateral force of rear tires.

The yaw motion around z-axis can be expressed as

$$I_Z\dot{\gamma} = l_\mathrm{f}F_{\mathrm{fa}x}\sin\delta_\mathrm{f} + l_\mathrm{f}F_{\mathrm{fa}y}\cos\delta_\mathrm{f} - dF_{\mathrm{fb}y}\sin\delta_\mathrm{f} - l_\mathrm{r}F_{\mathrm{ra}y}, \quad (3)$$

where $F_{\mathrm{fb}y} = F_{2y} - F_{1y}$ is the differential lateral force of front tires, and is caused by the vertical load transfer effects, etc.

To consider the saturation of tire forces, the Fiala tire model [24], which is a high-fidelity model to provide the nonlinear tire behavior and shows the boundary of lateral tire-road friction limits, is used to express the lateral tire force as

$$F_{iy} = \begin{cases} c_i\tan\beta_i\left(\dfrac{c_i^2\left(\tan\beta_i\right)^2}{27\left(\mu_i F_{iz}\right)^2} - \dfrac{c_i\left|\tan\beta_i\right|}{3\mu_i F_{iz}} + 1\right) & |\beta_i| \le \beta_{\max,i} \\ \mu_i F_{iz} & |\beta_i| > \beta_{\max,i}, \end{cases} \quad (4)$$

where c_i is the cornering stiffness constant of tire i; μ_i denotes the lateral friction coefficient of tire i; $\beta_{\max,i}$ represents the maximum sideslip angle of tire i when the tire fully-sliding behavior occurs.

Moreover, the longitudinal tire force would occupy the capacity of the total tire-road friction limits, and the lateral friction coefficient can be expressed by

$$\mu_i = F_{iz}^{-1}\sqrt{(\mu F_{iz})^2 - (F_{ix})^2}, \quad (5)$$

where μ is the total tire-road friction coefficient.

To apply the nonlinear tire model (4), the lateral tire forces without reaching the friction limits can be described by

$$\begin{cases} F_{\mathrm{fa}y} = \left(c_\mathrm{f} + \Delta c_\mathrm{f}\right)\beta_\mathrm{f}, \\ F_{\mathrm{ra}y} = \left(c_\mathrm{r} + \Delta c_\mathrm{r}\right)\beta_\mathrm{r}, \end{cases} \quad (6)$$

where β_f and β_r are the equivalent sideslip angles of the front and rear tires, respectively; c_f and c_r are the equivalent cornering stiffness constants for the linear parts of the front and rear tires, respectively; Δc_f and Δc_r are the nonlinear parts and approximation errors for the cornering stiffnesses of the front and rear tires, respectively. Then, we have $c_\mathrm{f} = c_1 + c_2$, $c_\mathrm{r} = c_3 + c_4$, $\Delta c_\mathrm{f} = \Delta c_1 + \Delta c_2$ and $\Delta c_\mathrm{r} = \Delta c_3 + \Delta c_4$. On this basis, one has

$$\Delta c_i = \tan\beta_i\left(\frac{c_i^2(\tan\beta_i)^2}{27(\mu_i F_{iz})^2} - \frac{c_i\left|\tan\beta_i\right|}{3\mu_i F_{iz}}\right) + \tan\beta_i - \beta_\mathrm{f}. \quad (7)$$

Since β_i is bounded while the tire fully-sliding behavior occurs, it can be inferred that $|\Delta c_\mathrm{f}|$ and $|\Delta c_\mathrm{r}|$ are bounded by positive constants c_{mf} and c_{mr}, respectively.

The equivalent sideslip angles of the front and rear wheels can be calculated using the vehicle kinematics as

$$\beta_\mathrm{f} = \delta_\mathrm{f} - \beta - v_x^{-1}l_\mathrm{f}\gamma,\ \beta_\mathrm{r} = v_x^{-1}l_\mathrm{r}\gamma - \beta. \quad (8)$$

2) Vehicle Dynamics With Unsaturated Tire Force: The vehicle sideslip angle represents the offset between the vehicle heading direction and the actual velocity direction. The lateral speed and acceleration can be expressed as

$$\begin{cases} v_y = v_x\tan\beta \approx v_x\beta, \\ \dot{v}_y = \dot{v}_x\tan\beta + v_x\dot{\beta}\left(\cos^2\beta\right)^{-1} \approx \dot{v}_x\beta + v_x\dot{\beta}. \end{cases} \quad (9)$$

Considering $v_x \neq 0$, the vehicle dynamics can be given as

$$\dot{\beta} = \left[-1 + \left(l_\mathrm{r}c_\mathrm{r} - l_\mathrm{f}c_\mathrm{f}\right)\left(mv_x^2\right)^{-1}\right]\gamma - \left(c_\mathrm{f} + c_\mathrm{r}\right)\left(mv_x\right)^{-1}\beta + \left(c_\mathrm{f} + \Delta c_\mathrm{f} + F_{\mathrm{fa}x}\right)\left(v_x m\right)^{-1}\delta_\mathrm{f} + d_\beta, \quad (10)$$

$$\dot{\gamma} = \left(l_\mathrm{r}c_\mathrm{r} - l_\mathrm{f}c_\mathrm{f}\right)I_Z^{-1}\beta - \left(l_\mathrm{f}^2c_\mathrm{f} + l_\mathrm{r}^2c_\mathrm{r}\right)\left(I_Z v_x\right)^{-1}\gamma + \left[l_\mathrm{f}c_\mathrm{f} + \left(l_\mathrm{f}\Delta c_\mathrm{f} + l_\mathrm{f}F_{\mathrm{fa}x} - dF_{\mathrm{fb}y}\right)\right]I_Z^{-1}\delta_\mathrm{f} + d_\gamma, \quad (11)$$

where

$$d_\gamma = \left(l_\mathrm{r}\Delta c_\mathrm{r} - l_\mathrm{f}\Delta c_\mathrm{f}\right)I_Z^{-1}\beta - \left(l_\mathrm{f}^2\Delta c_\mathrm{f} + l_\mathrm{r}^2\Delta c_\mathrm{r}\right)\left(I_Z v_x\right)^{-1}\gamma + d_{\gamma 1},$$

$$d_\beta = \left[-d_v v_x^{-1} + c_a m^{-1}v_x - \left(v_x m\right)^{-1}\left(\Delta c_\mathrm{f} + \Delta c_\mathrm{r}\right), + \left(F_{\mathrm{fa}x} + F_{\mathrm{ra}x}\right)m^{-1}\right]\beta + \left(l_\mathrm{r}\Delta c_\mathrm{r} - l_\mathrm{f}\Delta c_\mathrm{f}\right)\left(mv_x^2\right)^{-1}\gamma + d_{\beta 1},$$

while $d_{\beta 1}$ and $d_{\gamma 1}$are the unmodeled and perturbation items.

Remark 1: Considering the wheel dynamics, the longitudinal tire force in (10) and (11) can be calculated by

$$F_{xi} = R^{-1}\left(T_i - I_\mathrm{w}\dot{\omega}_i\right) + d_F, \quad (12)$$

where T_i is the effective torque on wheel i, I_w is the wheel's moment of inertia, and d_F incorporates the unknown tire slip and other traction losses.

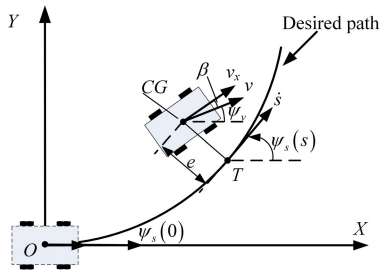

Fig. 2. Path Following Model.

From (12), we can find that the effective torque cannot be directly transferred to the wheel and produce the longitudinal tire force due to the wheel dynamics and traction losses. In real applications, the longitudinal tire force is always employed to control the longitudinal vehicle motion, whereas it also exists in the lateral vehicle dynamics as shown in (10) and (11). Thus, to perform the compensation of the wheel dynamics and the unexpected longitudinal tire force in the lateral vehicle dynamics, the items with $F_{\mathrm{fa}x}$ before the steering input δ_{f} in (10) and (11), together with the items with Δc_{f} and $F_{\mathrm{fb}y}$, are considered as the input faults, and a fault tolerant controller will be developed in this paper. In addition, the effects of the wheel dynamics and load transfer are also included in d_β and d_γ as the model uncertainties and disturbances.

Remark 2: In the path-following controller design, the sideslip angle of the vehicle is a significant parameter for the compensation of the heading direction error, whereas it is difficult to obtain. To address this issue, many topics have discussed the estimation of the vehicle sideslip angle. Dual Kalman filters are effective to perform the sensor fusing framework, and the vehicle sideslip angle can be accurately obtained by combining measurements of the magnetometer, global positioning system (GPS), and inertial measurement unit (IMU) [28]. Based on readily available inertial measurements, the industrially amenable approach based on the kinematic model shows satisfactory performance of the vehicle sideslip angle estimation [29]. Meanwhile, by integrating the tire model and the vehicle kinematics, the corner-based estimator can monitor the tire capacities and vehicle states [30]. In addition, the cyber-physical approach combined with the fault-tolerant estimation policy can be considered to obtain the other vehicle states [31]. Resorting to the above existing approaches, it is assumed that the vehicle states are known in this study.

B. Path Following Model

As an autonomous vehicle is supposed to follow a desired path, as shown in Fig. 2, the main target of the path-following controller is to stabilize the offset errors between the actual trajectory and the given path, including the velocity direction offset error ψ between the actual velocity direction ψ_v and the tangent direction of the given path ψ_s, and the distance offset error from the center of gravity of the vehicle to the orthogonal projection point T on the given path. As a result, since the actual trajectory cannot perfectly match the desired path, the vehicle and the projection point speeds are different. Then, the speed of the vehicle projection point on the given path can be given by

$$v_s = \dot{s} = [1 - e\kappa(s)]^{-1} \left(v_x \cos\psi - v_y \sin\psi\right) \approx v_x (1 - e\kappa)^{-1}, \tag{13}$$

where e is the distance offset error, and κ is the curvature of the desired path.

By using Serret-Frenet equation [32], the path-following errors dynamics can be written as

$$\begin{cases} \dot{e} = v_x \sin\psi + v_y \cos\psi \approx v_x \psi + v_x \beta, \\ \dot{\psi} = \dot{\psi}_v - \dot{\psi}_s \approx \gamma - \kappa(s) v_x + \dot{\beta}. \end{cases} \tag{14}$$

According to the vehicle model (10)-(11) and the path-following model (13)-(14), the ASM-FTC strategy will be designed to stabilize the path-following errors to zero while the tire force are not saturated. Furthermore, the additionally saturation control scheme will be designed by using the nonlinear tire model (4) and the vehicle motions (1)-(3).

III. Control System Design

A. Path Following Controller Design

To track desired paths, the path-following controller for the autonomous vehicle is proposed to stabilize the offset errors ψ and e to zero. To evaluate the path-following performance, choose the preview error [33] σ as

$$\sigma = e + \psi L, \tag{15}$$

where L is the preview length. Through converging the preview error σ to zero, the control objective can be achieved.

The time derivative of σ is given by

$$\dot{\sigma} = v_x \psi + v_x \beta + L\gamma - L\kappa v_x + \dot{\beta}. \tag{16}$$

Since the steering input is not implicitly in (16), taking the second-order time derivative of σ gives

$$\ddot{\sigma} = \dot{v}_x(\psi + \beta - L\kappa) - L\dot{\kappa} v_x - \kappa v_x^2 + v_x \gamma + 2v_x \dot{\beta} + L\dot{\gamma} + \ddot{\beta}. \tag{17}$$

Taking (10) and (11) into (17) produces

$$\begin{aligned} \ddot{\sigma} = {} & \underbrace{-L\dot{\kappa} v_x - \kappa v_x^2 - v_x \gamma}_{g_1} \\ & + [\underbrace{-\left(2m^{-1} + Ll_{\mathrm{f}} I_Z^{-1}\right) c_{\mathrm{f}}}_{g_2} \underbrace{- \left(2m^{-1} - Ll_{\mathrm{r}} I_Z^{-1}\right) c_{\mathrm{r}}}_{g_3}]\beta \\ & + [\underbrace{\left(2m^{-1} - Ll_{\mathrm{r}} I_Z^{-1}\right) c_{\mathrm{r}}}_{g_3} \frac{l_{\mathrm{r}}}{v_x} \underbrace{- \left(2m^{-1} + Ll_{\mathrm{f}} I_Z^{-1}\right) c_{\mathrm{f}}}_{g_2} \frac{l_{\mathrm{f}}}{v_x}]\gamma \\ & + \underbrace{\left(Ll_{\mathrm{f}} I_Z^{-1} + 2m^{-1}\right) c_{\mathrm{f}}}_{g_2} i_{\mathrm{f}} u + \underbrace{2v_x d_\beta + Ld_\gamma + \ddot{\beta}}_{d_g} \\ & + \underbrace{\left[L\left(l_{\mathrm{f}} \Delta c_{\mathrm{f}} + l_{\mathrm{f}} F_{\mathrm{fa}x} - d F_{\mathrm{fb}y}\right) I_Z^{-1} + 2\left(\Delta c_{\mathrm{f}} + F_{\mathrm{fa}x}\right) m^{-1}\right]}_{g_4} \\ & \times i_{\mathrm{f}} u \\ = {} & g_1 + (-g_2 - g_3)\beta + \left(g_3 \frac{l_{\mathrm{r}}}{v_x} - g_2 \frac{l_{\mathrm{f}}}{v_x}\right)\gamma + g_2 \delta_{\mathrm{f}} + g_4 \delta_{\mathrm{f}} \\ & + d_g, \end{aligned} \tag{18}$$

where i_{f} is the steering ratio from the steering wheel to the front wheels, and u is the steering angle of the steering wheel.

Select the preview length as

$$L = 2I_Z \left(l_{\mathrm{r}} m\right)^{-1}. \tag{19}$$

Substituting (19) into (18) yields

$$\ddot{\sigma} = g_1 - g_2\beta - g_2 l_{\mathrm{f}} v_x^{-1}\gamma + g_2\delta_{\mathrm{f}} + g_4\delta_{\mathrm{f}} + d_g. \tag{20}$$

This implies that g_3 has been cancelled out, and the preview length defined by (19) can effectively simplify the path-following controller calculations in the following sections.

Remark 3: The preview length defined by (19) is the distance from the center of gravity to the center of percussion [33], in which the preview error only depends on the front-tire force, as given in (20). The cornering stiffness of the rear tires is not included in (20). Therefore, the path-following controller does not require the knowledge of the rear-tire forces, and this will facilitate to analyze the tire force saturation.

Before giving the proposed controller, the following assumptions on the unknown disturbances are required.

Assumption 1: There exist positive constants d_1, d_2, and d_3, such that

$$\left|v_x d_\beta + L d_\gamma + \ddot{\beta}\right| \le d_1|\beta| + d_2|\gamma| + d_3. \tag{21}$$

Assumption 2: There exist a positive constant ε, such that

$$|g_4/g_2| \le \varepsilon < 1. \tag{22}$$

Remark 4: Since the vehicle moving environment is constantly changing and has finite energy, the disturbances and model errors, d_β and d_γ, of the vehicle system can be viewed as the unknown time-varying yet bounded items. In (10) and (11), d_β and d_γ include the vehicle states β and γ with bounded parameters. Meanwhile, $\ddot{\beta}$ is bounded. Therefore, the linear combination of d_β, d_γ, and $\ddot{\beta}$ can be bounded by the states and constants with positive scalars.

Remark 5: g_2 and g_4 represent the nominal effectiveness parameter and the uncertain faulty parameter of the actuator, respectively. Assumption 2 implies that the effective input is always larger than the input fault, and can dominate the actuator. In addition, it can be easily inferred that g_2 is positive.

Then, we are now ready to give the first result of this paper.

Theorem 1: Suppose the path-following controller as

$$u = -i_{\mathrm{f}}^{-1} g_2^{-1}\left(u_1 + u_2\right), \tag{23}$$

with

$$\begin{cases} u_1 = \sigma + g_5 - g_2\beta - l_{\mathrm{f}} v_x^{-1} g_2\gamma \\ u_2 = \left(d_1|\beta| + d_2|\gamma| + d_3 + \eta\right)\mathrm{sgn}(z), \end{cases} \tag{24}$$

where

$$\begin{cases} g_5 = k_1\left(v_x\psi + v_x\beta + L\gamma - L\kappa v_x\right) + g_1, \\ \lambda_1 = |u_1| + d_1|\beta| + d_2|\gamma| + d_3 + \lambda_2, \\ \lambda_3 = 1/(1-\varepsilon), \\ \eta = \left(\lambda_3 - 1\right)\lambda_1, \end{cases} \tag{25}$$

while k_1 and λ_2 are positive control gains. Then, the preview error is asymptotically stable.

Proof: Consider the Lyapunov function candidate

$$V_1 = \sigma^2/2. \tag{26}$$

The time derivative of V_1 is

$$\dot{V}_1 = \sigma\dot{\sigma} = \sigma\left(-k_1\sigma + z\right), \tag{27}$$

where $z = k_1\sigma + \dot{\sigma}$, and k_1 is a positive constant. Then, if $z = 0$, σ will be stabilized to the origin.

Taking time derivative of z yields

$$\begin{aligned} \dot{z} = \underbrace{k_1\left(v_x\psi + v_x\beta + L\gamma - L\kappa v_x\right) + g_1}_{g_5} - g_2\beta - g_2 l_{\mathrm{f}} v_x^{-1}\gamma \\ + g_2 i_{\mathrm{f}} u + g_4 i_{\mathrm{f}} u + d_g. \end{aligned} \tag{28}$$

Considering z, the Lyapunov function is rewritten as

$$V_2 = V_1 + z^2/2. \tag{29}$$

Invoking Assumption 1 and the controller (23), the time derivative of V_2 can be given by

$$\begin{aligned} \dot{V}_2 &\le -k_1\sigma^2 + |z|\left(d_1|\beta| + d_2|\gamma| + d_3\right) - z u_2 + z g_4 i_{\mathrm{f}} u \\ &= -k_1\sigma^2 - \eta|z| + z g_4 i_{\mathrm{f}} u. \end{aligned} \tag{30}$$

Considering the actuator fault in Assumption 2, we have

$$\begin{aligned} z g_4 i_{\mathrm{f}} u &\le \varepsilon|z|\underbrace{\left(|u_1| + d_1|\beta| + d_2|\gamma| + d_3 + \lambda_2\right)}_{\lambda_1} - \lambda_2 + \eta) \\ &= \varepsilon|z|\left(\lambda_1\lambda_3 - \lambda_2\right), \end{aligned} \tag{31}$$

where λ_1 and λ_2 are positive constants; λ_3 and η are constructed by $(1-\varepsilon)\lambda_3 = 1$ and $\eta = (\lambda_3 - 1)\lambda_1$, respectively.

Then, substituting (31) into (30) yields,

$$\begin{aligned} \dot{V}_2 &\le -k_1\sigma^2 + |z|\left[\varepsilon\left(\lambda_1\lambda_3 - \lambda_2\right) - \eta\right] \\ &= -k_1\sigma^2 + |z|\left\{\lambda_1\left[1 - (1-\varepsilon)\lambda_3\right] - \varepsilon\lambda_2\right\} \\ &= -k_1\sigma^2 - \varepsilon\lambda_2|z|, \end{aligned} \tag{32}$$

Thus, globally asymptotical stability of the closed-loop system can be guaranteed, that is, $\sigma \to 0$ as $t \to \infty$. The proof is completed. ■

B. Adaptive Controller Design With Unknown Parameters

From the controller design in Theorem 1, the upper bounds of the uncertain items given by Assumptions 1 and 2 need to be known to ensure the controlled system in a robust and stable situation. However, in real applications, it is difficult to obtain the accurate upper bounds of the perturbations and actuator faults. Moreover, high chattering and energy wastes may exhibit in the actuator if overlarge parameters are selected for the controller to overcome the unknown disturbances. Meanwhile, the steering ratio i_{f} is difficult to accurately measure. Therefore, this necessitates the deployment of adaptive techniques, as we shall present later.

In the following theorem, the control solution to the problem with unknown boundaries of the disturbances and actuator faults, as well as the unknown steering ratio, will be developed to stabilize the preview error by incorporating the adaptive sliding-mode fault-tolerant control action.

Theorem 2: Suppose the following adaptive sliding-mode fault-tolerant control law

$$u = -\hat{i}_{\mathrm{f}} g_2^{-1} \left(u_1 + u_2\right), \tag{33}$$

with

$$\begin{cases} u_1 = \sigma + g_5 - g_2\beta - g_2 l_{\mathrm{f}} v_x^{-1}\gamma, \\ u_2 = \left(\hat{d}_1|\beta| + \hat{d}_2|\gamma| + \hat{d}_3 + \hat{\eta}\right) \mathrm{sgn}\left(z_1\right), \end{cases} \tag{34}$$

updated by

$$\begin{cases} \dot{\hat{d}}_1 = p_1|z|\|\beta|, \\ \dot{\hat{d}}_2 = p_2|z|\|\gamma|, \\ \dot{\hat{d}}_3 = p_3|z|, \end{cases} \quad \begin{cases} \dot{\hat{i}}_{\mathrm{f}} = p_4 \hat{i}_{\mathrm{f}}^3 \left[z u_1 + |z| \left(\hat{d}_1|\beta| + \hat{d}_2|\gamma| + \hat{d}_3\right)\right], \\ \hat{\lambda}_1 = |u_1| + \hat{d}_1|\beta| + \hat{d}_2|\gamma| + \hat{d}_3 + \lambda_2 \\ \dot{\hat{\lambda}}_3 = p_5 \hat{\lambda}_1 \hat{i}_{\mathrm{f}}|z|, \\ \hat{\eta} = \left(\hat{\lambda}_3 - 1\right)\hat{\lambda}_1, \end{cases} \tag{35}$$

where $k_1, \lambda_2, p_1, p_2, p_3$ and p_4 are positive control gains. Then, the preview error is asymptotically stable.

Proof: Consider the following Lyapunov function candidate

$$V_3 = V_2 + \frac{\tilde{d}_1^2}{2p_1} + \frac{\tilde{d}_2^2}{2p_2} + \frac{\tilde{d}_3^2}{2p_3} + \frac{\tilde{i}_{\mathrm{f}}^2}{2p_4} + \frac{(1-\varepsilon)g_2}{2p_5}\tilde{\lambda}_3^2, \tag{36}$$

where $\tilde{d}_1 = d_1 - \hat{d}_1$, $\tilde{d}_2 = d_2 - \hat{d}_2$, $\tilde{d}_3 = d_3 - \hat{d}_3$, $\tilde{i}_{\mathrm{f}} = i_{\mathrm{f}} - \hat{i}_{\mathrm{f}}^{-1}$, $\tilde{\lambda}_3 = \lambda_3 - \hat{\lambda}_3$, and parameter λ_3 is a positive constant defined in (25). In addition, d_1, d_2, d_3, g_2 and λ_3 are all positive parameters, meanwhile, p_1, p_2, p_3, p_4 and p_5 are all positive control gains. Invoking Assumption 2, since $(1-\varepsilon)$ and g_2 are all positive, V_3 is always positive definite.

Taking time derivative of V_3 gives,

$$\begin{aligned} \dot{V}_3 &= -k_1\sigma^2 - p_1^{-1}\tilde{d}_1\dot{\hat{d}}_1 - p_2^{-1}\tilde{d}_2\dot{\hat{d}}_2 - p_3^{-1}\tilde{d}_3\dot{\hat{d}}_3 \\ &\quad + z[\underbrace{\sigma + g_5 - g_2\beta - g_2 l_{\mathrm{f}} v_x^{-1}\gamma}_{u_1} + g_2 i_{\mathrm{f}} u + g_4 i_{\mathrm{f}} u + d_g] \\ &\quad + p_4^{-1}\tilde{g}_2\hat{g}_2^{-2}\dot{\hat{g}}_2 - p_5^{-1}(1-\varepsilon)g_2\tilde{\lambda}_3\dot{\hat{\lambda}}_3 \\ &\le -k_1\sigma^2 + z\left(1 - i_{\mathrm{f}}\hat{i}_{\mathrm{f}}\right)u_1 + |z|\left(1 - i_{\mathrm{f}}\hat{i}_{\mathrm{f}}\right) \\ &\quad \left(\hat{d}_1|\beta| + \hat{d}_2|\gamma| + \hat{d}_3\right) + g_4 i_{\mathrm{f}} u z - p_1^{-1}\tilde{d}_1\dot{\hat{d}}_1 \\ &\quad + |z|\left(\tilde{d}_1|\beta| + \tilde{d}_2|\gamma| + \tilde{d}_3\right) - i_{\mathrm{f}}\hat{i}_{\mathrm{f}}\hat{\eta}|z| - p_2^{-1}\tilde{d}_2\dot{\hat{d}}_2 \\ &\quad - p_3^{-1}\tilde{d}_3\dot{\hat{d}}_3 + p_4^{-1}\tilde{i}_{\mathrm{f}}\hat{i}_{\mathrm{f}}^{-2}\dot{\hat{i}}_{\mathrm{f}} - p_5^{-1}(1-\varepsilon)g_2\tilde{\lambda}_3\dot{\hat{\lambda}}_3 \\ &= -k_1\sigma^2 + p_1^{-1}\tilde{d}_1\left(p_1|z||\beta| - \dot{\hat{d}}_1\right) + p_4^{-1}\tilde{i}_{\mathrm{f}}\hat{i}_{\mathrm{f}}^{-2} \\ &\quad \times \left\{\dot{\hat{i}}_{\mathrm{f}} - p_4\hat{i}_{\mathrm{f}}^3\left[z u_1 + |z|\left(\hat{d}_1|\beta| + \hat{d}_2|\gamma| + \hat{d}_3\right)\right]\right\} \\ &\quad + p_3^{-1}\tilde{d}_3\left(p_3|z| - \dot{\hat{d}}_3\right) - i_{\mathrm{f}}\hat{i}_{\mathrm{f}}\hat{\eta}|z| + g_4 i_{\mathrm{f}} u z \\ &\quad + p_2^{-1}\tilde{d}_2\left(p_2|z||\gamma| - \dot{\hat{d}}_2\right) - p_5^{-1}(1-\varepsilon)g_2\tilde{\lambda}_3\dot{\hat{\lambda}}_3 \\ &= -k_1\sigma^2 - i_{\mathrm{f}}\hat{i}_{\mathrm{f}}\hat{\eta}|z| + g_4 i_{\mathrm{f}} u z - p_5^{-1}(1-\varepsilon)g_2\tilde{\lambda}_3\dot{\hat{\lambda}}_3. \end{aligned} \tag{37}$$

Considering the actuator fault, we have,

$$\begin{aligned} g_4 i_{\mathrm{f}} u z &\le \varepsilon i_{\mathrm{f}}\hat{i}_{\mathrm{f}}|z|(\underbrace{|u_1| + \hat{d}_1|\beta| + \hat{d}_2|\gamma| + \hat{d}_3 + \lambda_2}_{\hat{\lambda}_1} - \lambda_2 + \hat{\eta}) \\ &= \varepsilon i_{\mathrm{f}}\hat{i}_{\mathrm{f}}|z|\left(\hat{\lambda}_1\hat{\lambda}_3 - \lambda_2\right), \end{aligned} \tag{38}$$

where $\hat{\eta} = \lambda_1\left(\hat{\lambda}_3 - 1\right)$.

Substituting (38) into (37) produces

$$\begin{aligned} \dot{V}_3 &\le -k_1\sigma^2 + \varepsilon i_{\mathrm{f}}\hat{i}_{\mathrm{f}}|z|\left(\hat{\lambda}_1\hat{\lambda}_3 - \lambda_2\right) - i_{\mathrm{f}}\hat{i}_{\mathrm{f}}\hat{\eta}|z| \\ &\quad - p_5^{-1}(1-\varepsilon)i_{\mathrm{f}}\tilde{\lambda}_3\dot{\hat{\lambda}}_3 \\ &= i_{\mathrm{f}}\hat{i}_{\mathrm{f}}\hat{\lambda}_1|z|\left(\varepsilon\hat{\lambda}_3 - \hat{\lambda}_3 + 1\right) - p_5^{-1}(1-\varepsilon)i_{\mathrm{f}}\tilde{\lambda}_3\dot{\hat{\lambda}}_3 \\ &\quad - \lambda_2\varepsilon i_{\mathrm{f}}\hat{i}_{\mathrm{f}}|z| - k_1\sigma^2 \\ &= i_{\mathrm{f}}\hat{i}_{\mathrm{f}}\lambda_1|z|(1-\varepsilon)\tilde{\lambda}_3 - p_5^{-1}(1-\varepsilon)i_{\mathrm{f}}\tilde{\lambda}_3\dot{\hat{\lambda}}_3 \\ &\quad - \lambda_2\varepsilon i_{\mathrm{f}}\hat{i}_{\mathrm{f}}|z| - k_1\sigma^2 \\ &= p_5^{-1}(1-\varepsilon)\tilde{\lambda}_3 g_2\left(p_5\lambda_1\hat{i}_{\mathrm{f}}\,|z_1| - \dot{\lambda}_3\right) \\ &\quad - \lambda_2\varepsilon i_{\mathrm{f}}\hat{i}_{\mathrm{f}}|z| - k_1\sigma^2 \\ &= -\lambda_2\varepsilon i_{\mathrm{f}}\hat{i}_{\mathrm{f}}|z| - k_1\sigma^2 \le -k_1\sigma^2 < 0, \quad \forall\sigma \ne 0, \end{aligned} \tag{39}$$

which implies that $\lim_{t\to\infty} V_3(t) = V_3(\infty)$ exists.

Integrating V_3 from 0 to ∞ yields

$$\lim_{t\to\infty}\int_0^t |\sigma(\tau)|\mathrm{d}\tau \le k^{-1}(V(0) - V(\infty)) \tag{40}$$

Since the term on the right-hand side is bounded, $\lim_{t\to\infty}\sigma = 0$ can be obtained using Barbalat's Lemma. Thus, globally asymptotical stability of the closed-loop system can be guaranteed, that is, $\sigma \to 0$ as $t \to \infty$. The proof is completed. ■

C. Path-Following Controller Design With Unknown Tire Force Saturation

From the practical perspective, the input generated by the designed control law in Theorem 2 might not be implemented in the vehicle system due to the tire-road friction limits. As depicted in Fiala nonlinear tire model (4), the lateral tire force is constrained by the available tire-road friction limits. To consider the saturated tire force, the lateral and yaw motions of the vehicle can be rewritten by using (1)-(3) as

$$\begin{cases} \dot{\beta} = -\gamma + \dfrac{1}{m v_x}\left[\mathrm{sat}\left(F_{\mathrm{fay}}\right) + \mathrm{sat}\left(F_{\mathrm{ray}}\right)\right] + d_\beta \\ \dot{\gamma} = \dfrac{1}{I_z}\left[l_{\mathrm{f}}\mathrm{sat}\left(F_{\mathrm{fay}}\right) - l_{\mathrm{r}}\mathrm{sat}\left(F_{\mathrm{ray}}\right)\right] + d_\gamma, \end{cases} \tag{41}$$

where $\mathrm{sat}\left(F_{\mathrm{fay}}\right) = \mathrm{sgn}\left(F_{\mathrm{fay}}\right)\min\left\{\left|F_{\mathrm{fax}}\right|, F_{\mathrm{ymax}}\right\}$, $\mathrm{sat}\left(F_{\mathrm{ray}}\right) = \mathrm{sgn}\left(F_{\mathrm{ray}}\right)\min\left\{\left|F_{\mathrm{ray}}\right|, F_{\mathrm{ymax}}\right\}$ and $F_{x\mathrm{max}}$ is the available lateral tire-road friction limits. According to (8), the steering input can only control the front tire force F_{fay} while the tire is not saturated.

Invoking the position at the center of percussion in (19), the second-order time derivative of σ can be calculated by substituting (41) into (17) as follows

$$\ddot{\sigma} = g_1 + g_2\,\mathrm{sat}\left(F_{\mathrm{fay}}\right) + g_4\,\mathrm{sat}\left(F_{\mathrm{fay}}\right) + d_g. \tag{42}$$

Then, we are going to give the last result of this paper.

Theorem 3: Considering the actuator fault and the saturated tire force, the modified path-following control law is designed as

$$u = u_0 - k_2\, z, \tag{43}$$

where k_2 is a positive control gain, and u_0 is the same controller designed in Theorem 2. Then, the preview error is asymptotically stable.

Proof: Invoking (8), substituting the modified controller (43) into (4) yields

$$\begin{aligned}\text{sat}\left(F_{\text{fay}}\right) &= \text{sat}\left\{c_{\text{f}}\left[i_{\text{f}}\left(u_0 - k_2 z\right) - \beta - l_{\text{f}} v_x^{-1}\gamma\right]\right\} \\ &= \text{sat}[\underbrace{c_{\text{f}}\left(i_{\text{f}} u_0 - \beta - l_{\text{f}} v_x^{-1}\gamma\right)}_{F_{y0}} - k_2 i_{\text{f}} c_{\text{f}} z], \\ &= F_{y0} - \underbrace{\left[\text{sat}\left(k_2 i_{\text{f}} c_{\text{f}} z - F_{y0}\right) + F_{y0}\right]}_{F_u}\end{aligned} \tag{44}$$

where F_{y0} is the lateral force of front wheels produced by the control law u_0.

Note that

$$F_u = \begin{cases} k_2 i_{\text{f}} z, & \text{if } \left|k_2 i_{\text{f}} z - F_{y0}\right| \le F_{y\max} \\ F_{y\max} + F_{y0}, & \text{if } k_2 i_{\text{f}} z - F_{y0} > F_{y\max} \\ -F_{y\max} + F_{y0}, & \text{if } k_2 i_{\text{f}} z - F_{y0} < -F_{y\max}, \end{cases} \tag{45}$$

For the path-following performance in the control law with the consideration of tire force saturation, an estimated domain of attraction of the origin can be determined using the Lyapunov function V_3 as [34]

$$D\left(b_\sigma\right) = \left\{\sigma \in \mathbb{R} \mid V_3 \le b_\sigma\right\}, \tag{46}$$

where $D\left(b_\sigma\right)$ is a contractively invariant set, and b_σ is selected such that

$$\max_{\sigma \in D(b_\sigma)} \left|F_{\text{fay}}\right| \le F_{y\max}. \tag{47}$$

To improve the convergence speed within the contractively invariant set $D\left(b_\sigma\right)$, the Lyapunov function in (36), together with (42), (44) and (45), can be modified by

$$\begin{aligned}\dot{V}_3 &= -k\sigma^2 - \left(g_2 + g_4\right) z F_u \\ &= -k\sigma^2 \\ &\quad - \begin{cases} \left(g_2 + g_4\right) k_2 i_{\text{f}} i^2, & \left|k_2 i_{\text{f}} i z - F_{y0}\right| \le F_{y\max} \\ \left(g_2 + g_4\right) z\left(F_{y\max} + F_{y0}\right), & \\ \left(k_2 i_{\text{f}} i z - F_{y0}\right) > F_{y\max} & \\ \left(g_2 + g_4\right) z\left(-F_{y\max} + F_{y0}\right), & \\ \left(k_2 i_{\text{f}} i z - F_{y0}\right) < -F_{y\max} & \end{cases}\end{aligned} \tag{48}$$

Invoking Assumption 2 and (45), $g_2 + g_4$ is positive, and $\dot{V}_3 < 0$ for $\sigma \in D\left(b_\sigma\right)$. Resorting to the Barbalat's Lemma, it can be obtained that the preview error can be stabilized to zero. This completes the proof. ■

Remark 6: From the proposed saturation controller in Theorem 3, an additional component is given to improve the closed-loop response while the inputted tire force is saturated. We notice that no boundaries of the saturation item are required in the saturation component, and the prior knowledge of the tire-road friction coefficient is also non-essential.

TABLE II
MAIN PARAMETERS FOR VEHICLE MODEL

Symbol	Value	Symbol	Value
m	1230 kg	I_Z	1343 kg·m^2
l_{f}	1.04 m	c_{f}	96300 N/rad
l_{r}	1.56 m	c_{r}	64200 N/rad
d	0.79 m	R	0.3 m

D. Conventional Sliding-Mode Controller

To compare with the proposed controller, we construct a conventional sliding-mode controller to follow the desired paths. Select the following sliding-mode surface

$$S = \sigma + k_s \dot{\sigma}, \tag{49}$$

where k_s is the positive control gain. As indicated in (49), the preview error σ can be stabilized as S is converged to zero.

According to the sliding-mode algorithm without the consideration of the input fault and tire force saturation, the following controller can be used to stabilize S to zero

$$\begin{aligned}u = &-\left(k_s g_2 i_{\text{f}}\right)^{-1} \dot{\sigma} - \left(g_2 i_{\text{f}}\right)^{-1} \\ &\left(g_1 - g_2\beta - g_2 l_{\text{f}} v_x^{-1}\gamma + d_4\,\text{sgn}(S)\right),\end{aligned} \tag{50}$$

where d_4 is the upper bound of the unknown perturbation in the path-following system. Then, by using the conventional sliding-mode controller (50), the preview error can be stabilized to the origin.

IV. SIMULATION RESULTS

In this section, the ASM-FTC strategy with consideration of the lateral tire-road force saturation (Saturation Controller, SC), the ASM-FTC strategy without consideration of the saturated tire force (Normal Controller, NC), and the conventional sliding-mode controller without consideration of the input fault and tire force saturation (Conventional Controller, CC) are conducted on CarSim-Simulink platform with the high-fidelity vehicle model, which incorporates the nonlinear tire model with uncertainties and disturbances. In the simulation implementation, U-turn and S-curve with different tire-road friction coefficients and vehicle speeds are adopted to verify the effectiveness of the proposed saturation control strategy. The vehicle parameters for the simulations are listed in Table II, and the parameters for the controllers are chosen in Table III.

To conduct continuous steering inputs, the desired paths are required to have continuous curvatures, and thereby clothoids, which are described by linearly varying curvatures along its length, have been widely used to plan path and design road. Thus, the clothoid curves of U-turn and S-curve are used for the desired paths, and the curvatures are shown in Fig. 3.

TABLE III
CONTROLLER PARAMETERS

Controller	Value
Normal Controller	$k_1 = 30, \lambda_2 = 1$ $p_1 = p_2 = p_3 = 0.001, p_4 = 10^{-8}, p_5 = 10^{-7}$
Saturation Controller	$k_1 = 30, \lambda_2 = 1, k_2 = 0.002$ $p_1 = p_2 = p_3 = 0.001, p_4 = 10^{-8}, p_5 = 10^{-7}$
Conventional Controller	$k_s = 0.15, d_4 = 1$

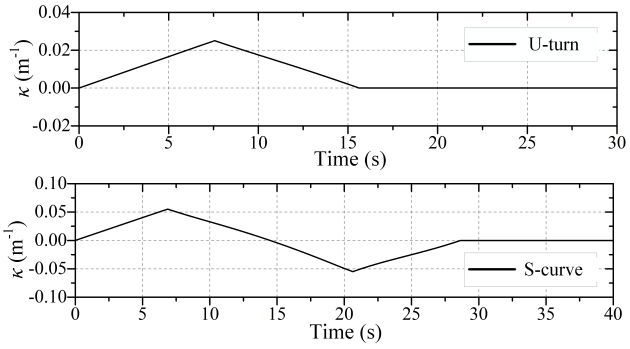

Fig. 3. Curvatures for desired paths.

A. S-Curve and U-Turn Simulations With Unsaturated Tire

In these two cases, the autonomous vehicle is within the tire-road friction limits. To verify the effectiveness of the three comparative controllers while the tire-road friction limits are not reached, the vehicle is driven at a low speed ($v_x = 30$ km/h) on a dry road with a high friction ($\mu = 0.85$). The simulation results are plotted in Fig. 4.

From the path-following trajectories in Figs. 4(a) and (b), either the saturation controller or the normal controller is more effective to follow the desired paths of S-curve and U-turn, compared with the conventional controller. Furthermore, in the time response of preview errors as shown in Figs. 4(c) and (d), it can be seen that the preview errors can be stabilized to near zero. Due to the neglect of input faults, we can find that the conventional controller exhibits the largest preview errors. Note that, the lateral accelerations of the controlled vehicle, as shown in Figs. 4(e) and (f), are able to increase while the curvatures of the desired paths increase, and thereby the tire-road forces are not saturated. As a result, one can observe that the saturation controller outperforms the normal and conventional controllers when the tire-road friction limits are not reached.

B. S-Curve With Saturated Tire

In this case, the tire of the autonomous vehicle would reach the friction limits, and the tire forces show saturation situation while the vehicle is driven on a slippery wet road. The conditions with a low friction ($\mu = 0.3$) and a low speed ($v = 30$ km/h) are implemented in the simulation. The autonomous vehicle is supposed to track an ideal S-curve with the curvature as shown in Fig. 3. By conducting the saturation,

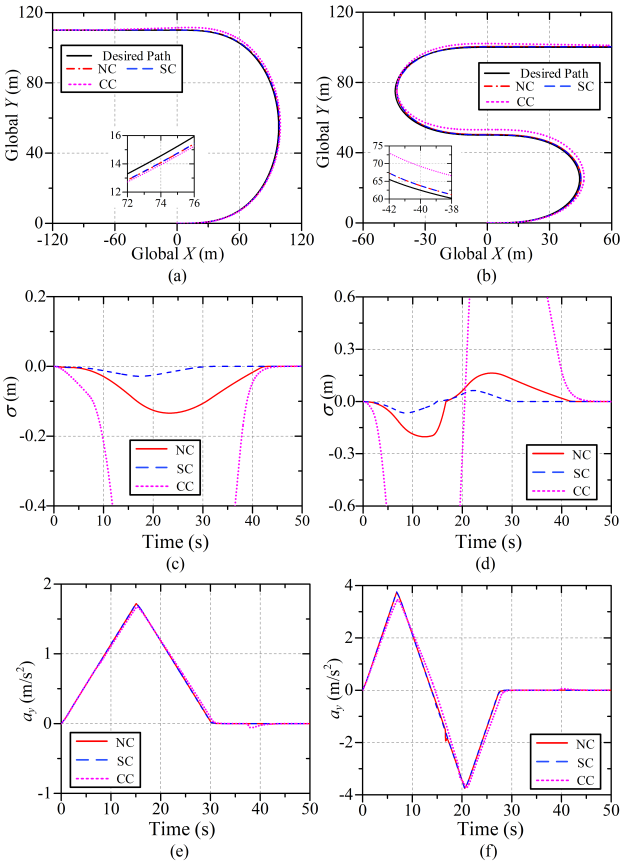

Fig. 4. Simulation results. (a) Path following trajectory for U-turn. (b) Path following trajectory for S-curve. (c) Preview error for U-turn. (d) Preview error for S-curve. (e) Lateral acceleration for U-turn. (f) Lateral acceleration for S-curve.

normal and conventional controllers, the simulation results are plotted in Fig. 5.

Due to the extremely slippery conditions while tire-road friction limits are reached, the autonomous vehicle controlled by the saturation, normal and conventional controllers exhibits large tracking offsets to follow the desired S-curve path, as shown in Fig 5(a), but can be finally driven back to the given path. From this result, we observe that the vehicle controlled by the saturation controller can be driven back to the desired path more quickly and accurately over the vehicle with the normal controller or the conventional controller. Furthermore, the time responses of the path-following errors, including the preview error, direction offset error and distance offset error, are shown in Figs. 5(b)-(d). It can be seen that the path-following errors can be finally stabilized to zero by the saturation and normal controllers. However, it requires more than 40s for the vehicle controlled by the normal controller, which is about 30s for the vehicle controlled by the saturation controller, to converge the path-following errors to near zero. Moreover, the conventional controller cannot drive the vehicle back to the desired path before 40s. As a result, the vehicle with the saturation controller has the best response performance to follow the desired path in the three comparative controllers. Note that, the direction error of the autonomous vehicle with the saturation controller, as shown in Fig. 5(c),

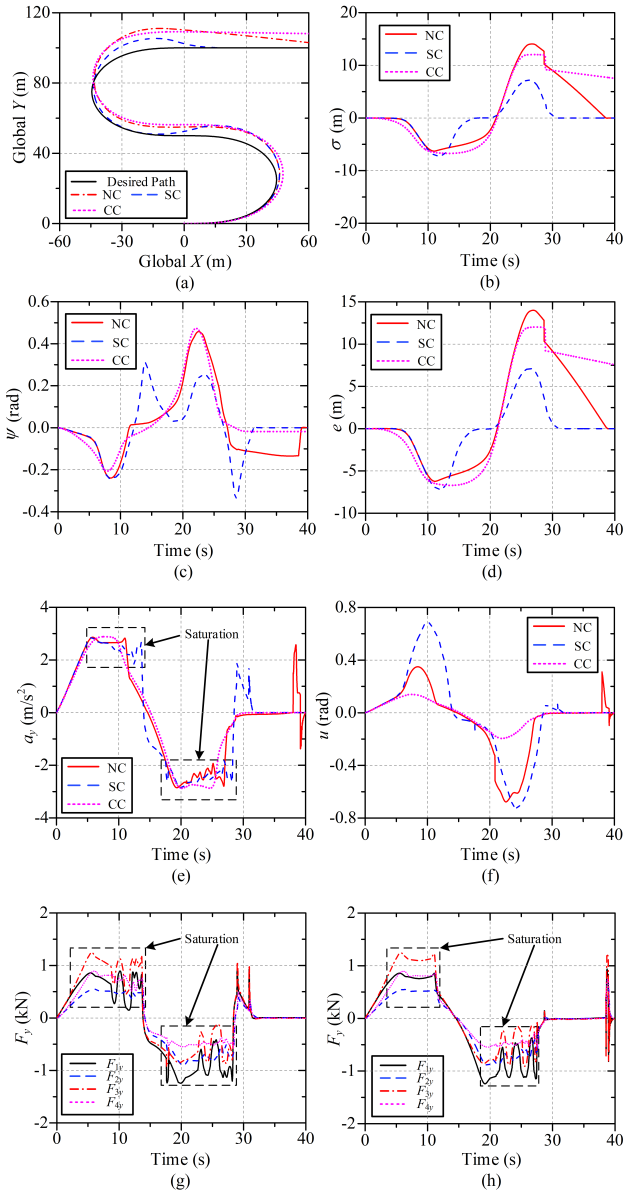

Fig. 5. Simulation results for S-curve. (a) Path-following trajectory. (b) Preview error. (c) Direction error. (d) Distance error. (e) Lateral acceleration. (f) Steering wheel input. (g) Lateral tire force using SC. (h) Lateral tire force using NC.

is higher compared with the vehicle controlled by the normal controller or the conventional controller during 25s to 30s. This can be explained by, together with the distance offset errors plotted in Fig. 5(e), the vehicle with the saturation controller can quickly response to change the direction to the desired path through sacrificing the direction match due to the large distance offset.

The lateral accelerations and the lateral tire forces are shown in Figs. 5(e), (g) and (h), from which, one can find that the lateral accelerations and the tire forces are not able to keep increasing while the curvature and the steering input increase. Therefore, it can be inferred that the tire-road friction reaches the limits under the conditions of the low friction and speed. Meanwhile, we notice that the lateral tire forces with the saturation controller stay in the saturated stage for the longest time compared with those of the normal and conventional controllers. This is because, the vehicle uses the largest steering inputs from the saturation controller, as shown in Fig. 5(f), to fully utilize the tire-road friction capacity to stabilize the path-following errors under the saturated conditions.

C. U-Turn With Saturated Tire

In this section, we present a U-turn simulation case implementation on CarSim-Simulink platform. To verify the proposed controllers in the simulation under the different conditions, the vehicle is supposed to run at a higher speed (v_x = 60 km/h) on a road with a medium tire-road friction coefficient ($\mu = 0.6$), such that the tire-road friction limits are reached.

The simulation results of the path-following trajectory are plotted in Fig. 6(a). This figure, together with the time responses of the path-following errors in Figs. 6(b)-(d), illustrates that the controlled vehicle with the saturation controller can always maintain the superior tracking accuracy and speed than the vehicle with the normal controller or the conventional controller, and the tracking performance has been effectively improved. Note that, the normal controller and the conventional controller are difficult to converge the preview error and the position error to near zero within 30 s. Furthermore, the proposed saturation control strategy can stabilize the preview and position errors to zero within 17 s. Similarly, the lateral accelerations and tire forces in Figs. 6(e), (g) and (h) exhibit tire-road force saturations.

We notice that, the vehicle controlled by the normal controller exhibit oscillations during 35 s to 40 s, as shown in Figs. 5(e) and (f). This is because, when the vehicle has just reached the desired path from the large offset position and the distance offset error has been converged to zero, the heading direction error is quickly rectified at about 40 s, as shown in Fig. 5(c). Similarly, the oscillations of the vehicle controlled by the saturation controller can also be found at about 30 s in Figs. 5(c), (e) and (f), and at about 15 s in Figs. 6(c), (e) and (f). Therefore, the fierce corrective steering inputs for the heading direction offset errors lead to the oscillation phenomena. To eliminate the oscillations, a re-planned path with continuous curvatures can be considered to ensure the smooth transition between the large offset position and the desired path while the vehicle has been away from the saturation region.

Even though the proposed "SC" controller always outperforms the comparative controllers, the vehicles controlled by the above-mentioned controllers all exhibit large distance offset errors, as shown in Figs. 5 and 6. This is because that, the extreme driving maneuvers, including the constant cornering speeds without braking, the persistent and large-scale saturations of the tire force, and the low frictions of the road surface (μ = 0.3 and 0.6), are implemented in CarSim platform. In real applications, such large distance offset errors are generally unacceptable due to the safety concern, and these extreme driving maneuvers cannot be practically operated on urban roads.

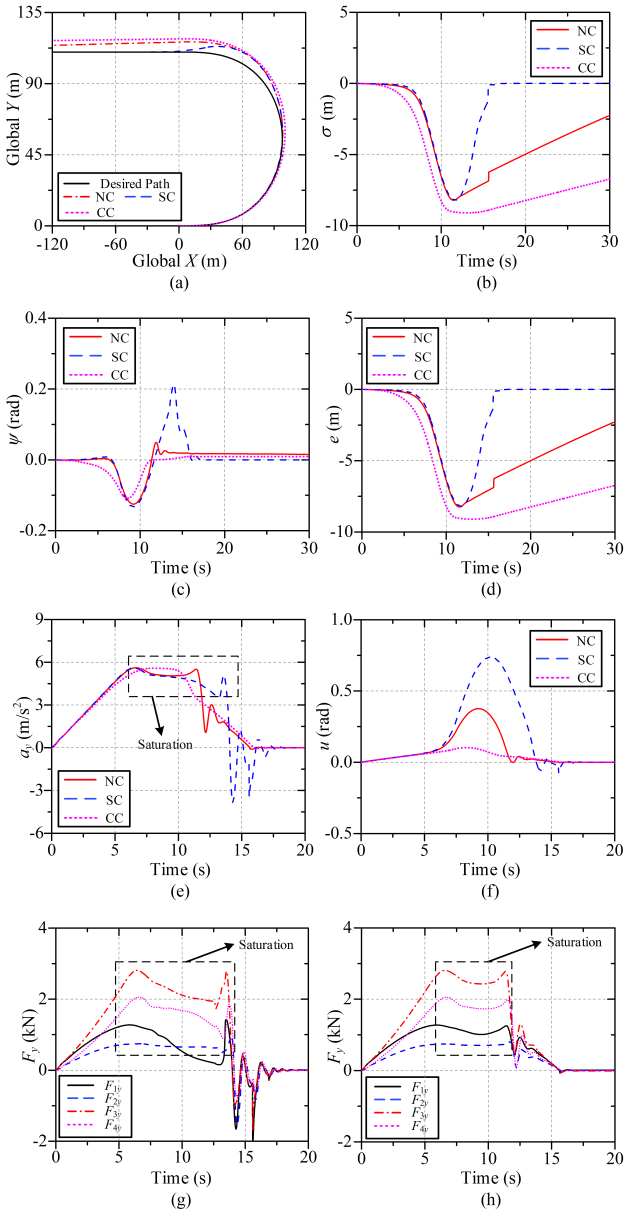

Fig. 6. Simulation results for U-turn. (a) Path-following trajectory. (b) Preview error. (c) Direction error. (d) Distance error. (e) Lateral acceleration. (f) Steering wheel input. (g) Lateral tire force using SC. (h) Lateral tire force using NC.

D. Composite Maneuvers With Saturated Tire

From the results in Figs. 5 and 6, one can find that, the distance offset errors exceed 6 m while the lateral tire force is saturated and the vehicle keeps constant speeds, and the controlled vehicle may crash to the road boundaries. To address this issue, we propose the composite maneuvers integrating the brake and steer operations to decelerate the controlled vehicle while the preview error exceeds a preset value. Furthermore, it is worth noting that, overlarge preview error implies the vehicle may approach to or has already been within the saturated tire force situation, and that the longitudinal tire braking force will also occupy a part of the available tire force capacity. Thus, the preview error will not be immediately reduced while the brake operation starts performing.

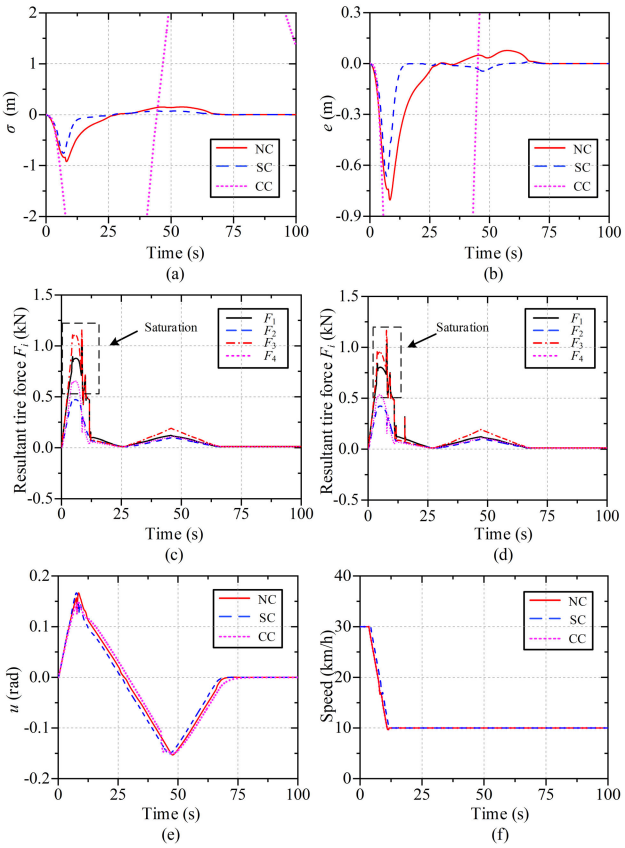

Fig. 7. Simulation results for S-curve in composite maneuvers. (a) Preview error. (b) Distance error. (c) Resultant of tire force using SC. (d) Resultant of tire force using NC. (e) Steering wheel input. (f) Vehicle speed.

Considering the maximum preview error results in Fig. 4 under the unsaturated tire force condition, the preset value for the preview error starting the brake operation is selected as 0.3 m. When the actual preview error exceeds 0.3 m, the brake operation starts to intervene. As a matter of fact, a smaller preset value can alternatively be applied for the proposed saturation controller to obtain better performance, and the common value of 0.3 m is selected for fair comparisons in this study. In addition, $k_1 = 4$ is set for the composite maneuvers. In the composite maneuvers, two different mechanisms are proposed to end the brake operation, i.e., the vehicle is decelerated to the preset lower bound of speed, and the preview error is stabilized below 0.25 m. Here, different starting and ending values for the preview error are introduced to avoid frequent brake operations. Finally, the vehicle restores to the constant speed.

In the composite maneuvers with the common lower bound of speed, the preview errors of vehicle controlled by the normal controller and the proposed saturation controller in the S-curve path can be significantly reduced, as shown in Fig. 7. Since the longitudinal tire braking force occupies a part of the available tire force capacity, the preview error and the distance offset error are not immediately reduced, as plotted in Figs. 7(a) and (b). Correspondingly, from Figs. 7(c) and (d), we can observe that the resultant tire forces are saturated during the initial few seconds. In comparison, the proposed saturation controller can provide superior path-following performance over the other comparative controllers.

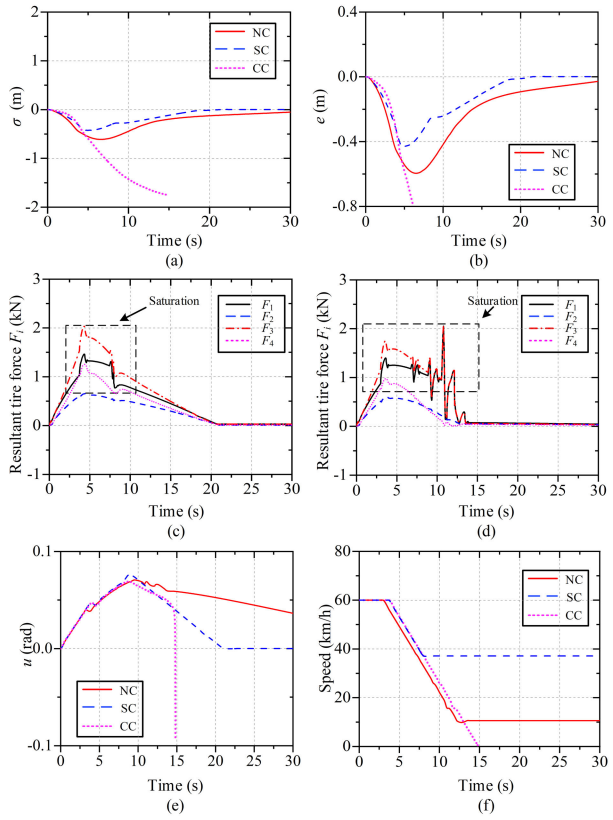

Fig. 8. Simulation results for U-turn in composite maneuvers. (a) Preview error. (b) Distance error. (c) Resultant of tire force using SC. (d) Resultant of tire force using NC. (e) Steering wheel input. (f) Vehicle speed.

In the composite maneuvers with the common lower bound of preview error, the proposed saturation controller outperforms the other comparative controllers, as shown in Fig. 8. In particular, the preview error fails to be confined below 0.25 m by the conventional controller before the vehicle stops, and the vehicle controlled by the normal controller is decelerated to a low speed, as shown 8(f). In contrast, the proposed saturation controller maintains the controlled vehicle at a higher speed, and achieves superior path-following performance.

Summarizing all the cases, including the unsaturated tire force cases and the saturated tire force cases, it is noted that the proposed saturation control scheme can significantly improve the path-following performance over the normal ASM-FTC without consideration of the saturation situations and the conventional sliding-mode method without consideration of the tire saturations and input faults in the CarSim-Simulink simulations. In the saturation cases, the proposed saturation approach shows the best path-following results, even in presence of unknown-bound disturbances and nonlinear model faults, unknown actuator parameters, and unknown tire-road friction coefficients.

V. Conclusion

In this paper, an adaptive sliding-mode fault-tolerant-control (ASM-FTC) strategy integrated with saturation algorithm is proposed to maintain the autonomous vehicle following desired paths as the boundaries of uncertainties and disturbances, the boundaries of actuator faults, the steering ratio from the steering wheel to the front wheels, and the tire-road friction constraints are all unknown. By selecting the distance from the center of gravity to the center of percussion as the preview length, the lateral force saturation of the rear tires can be cancelled and neglected in the preview error of the path-following model. On this basis, compared with the normal ASM-FTC and conventional sliding-mode strategies, the proposed ASM-FTC integrated with saturation control algorithm is more effective and fast to stabilize the preview error to zero with the constraints of the tire-road friction limits.

References

[1] Y. Xia, F. Pu, S. Li, and Y. Gao, "Lateral path tracking control of autonomous land vehicle based on ADRC and differential flatness," *IEEE Trans. Ind. Electron.*, vol. 63, no. 5, pp. 3091–3099, May 2016.

[2] X. He, Y. Liu, C. Lv, X. Ji, and Y. Liu, "Emergency steering control of autonomous vehicle for collision avoidance and stabilisation," *Vehicle Syst. Dyn.*, vol. 57, no. 8, pp. 1163–1187, Aug. 2019.

[3] J. Ni, J. Hu, and C. Xiang, "Envelope control for four-wheel independently actuated autonomous ground vehicle through AFS/DYC integrated control," *IEEE Trans. Veh. Technol.*, vol. 66, no. 11, pp. 9712–9726, Nov. 2017.

[4] X. Yuan, G. Huang, and K. Shi, "Improved adaptive path following control system for autonomous vehicle in different velocities," *IEEE Trans. Intell. Transp. Syst.*, vol. 21, no. 8, pp. 3247–3256, Aug. 2020.

[5] N. Guo, X. Zhang, Y. Zou, B. Lenzo, and T. Zhang, "A computationally efficient path-following control strategy of autonomous electric vehicles with yaw motion stabilization," *IEEE Trans. Transport. Electrific.*, vol. 6, no. 2, pp. 728–739, Jun. 2020.

[6] W. Zhang, Z. Wang, L. Drugge, and M. Nybacka, "Evaluating model predictive path following and yaw stability controllers for over-actuated autonomous electric vehicles," *IEEE Trans. Veh. Technol.*, vol. 69, no. 11, pp. 12807–12821, Nov. 2020.

[7] Z. Luan, J. Zhang, W. Zhao, and C. Wang, "Trajectory tracking control of autonomous vehicle with random network delay," *IEEE Trans. Veh. Technol.*, vol. 69, no. 8, pp. 8140–8150, Aug. 2020.

[8] H. Zhang and J. Wang, "Adaptive sliding-mode observer design for a selective catalytic reduction system of ground-vehicle diesel engines," *IEEE/ASME Trans. Mechatronics*, vol. 21, no. 4, pp. 2027–2038, Aug. 2016.

[9] Z. Liang, J. Chen, and Y. Wang, "Equivalent acceleration imitation for single wheel of manned lunar rover by varying torque on earth," *IEEE/ASME Trans. Mechatronics*, vol. 25, no. 1, pp. 282–293, Feb. 2020.

[10] Y. Yu, C. Guo, and H. Yu, "Finite-time PLOS-based integral sliding-mode adaptive neural path following for unmanned surface vessels with unknown dynamics and disturbances," *IEEE Trans. Autom. Sci. Eng.*, vol. 16, no. 4, pp. 1500–1511, Oct. 2019.

[11] Y. Wu, L. Wang, J. Zhang, and F. Li, "Path following control of autonomous ground vehicle based on nonsingular terminal sliding mode and active disturbance rejection control," *IEEE Trans. Veh. Technol.*, vol. 68, no. 7, pp. 6379–6390, Jul. 2019.

[12] Z. Liang, J. Zhao, Z. Dong, Y. Wang, and Z. Ding, "Torque vectoring and rear-wheel-steering control for vehicle's uncertain slips on soft and slope terrain using sliding mode algorithm," *IEEE Trans. Veh. Technol.*, vol. 69, no. 4, pp. 3805–3815, Apr. 2020.

[13] J. Chen, Z. Shuai, H. Zhang, and W. Zhao, "Path following control of autonomous four-wheel-independent-drive electric vehicles via second-order sliding mode and nonlinear disturbance observer techniques," *IEEE Trans. Ind. Electron.*, vol. 68, no. 3, pp. 2460–2469, Mar. 2021.

[14] J. Guo, Y. Luo, and K. Li, "An adaptive hierarchical trajectory following control approach of autonomous four-wheel independent drive electric vehicles," *IEEE Trans. Intell. Transp. Syst.*, vol. 19, no. 8, pp. 2482–2492, Aug. 2018.

[15] S. E. Li, H. Chen, R. Li, Z. Liu, Z. Wang, and Z. Xin, "Predictive lateral control to stabilise highly automated vehicles at tire-road friction limits," *Vehicle Syst. Dyn.*, vol. 58, no. 5, pp. 768–786, Jan. 2020.

[16] C. Hu et al., "MME-EKF-based path-tracking control of autonomous vehicles considering input saturation," *IEEE Trans. Veh. Technol.*, vol. 68, no. 6, pp. 5246–5259, Jun. 2019.

[17] J. Ni and J. Hu, "Dynamics control of autonomous vehicle at driving limits and experiment on an autonomous formula racing car," *Mech. Syst. Signal Process.*, vol. 90, pp. 154–174, Jun. 2017.
[18] E. Siampis, E. Velenis, S. Gariuolo, and S. Longo, "A real-time nonlinear model predictive control strategy for stabilization of an electric vehicle at the limits of handling," *IEEE Trans. Control Syst. Technol.*, vol. 26, no. 6, pp. 1982–1994, Nov. 2018.
[19] Z. Liang, J. Zhao, B. Liu, Y. Wang, and Z. Ding, "Velocity-based path following control for autonomous vehicles to avoid exceeding road friction limits using sliding mode method," *IEEE Trans. Intell. Transp. Syst.*, vol. 23, no. 3, pp. 1947–1958, Mar. 2022.
[20] C. Hu, Z. Wang, Y. Qin, Y. Huang, J. Wang, and R. Wang, "Lane keeping control of autonomous vehicles with prescribed performance considering the rollover prevention and input saturation," *IEEE Trans. Intell. Transp. Syst.*, vol. 21, no. 7, pp. 3091–3103, Jul. 2020.
[21] M. Jalali, E. Hashemi, A. Khajepour, S.-K. Chen, and B. Litkouhi, "A combined-slip predictive control of vehicle stability with experimental verification," *Vehicle Syst. Dyn.*, vol. 56, no. 2, pp. 319–340, Feb. 2018.
[22] E. Hashemi, M. Jalali, A. Khajepour, A. Kasaiezadeh, and S. Chen, "Vehicle stability control: Model predictive approach and combined-slip effect," *IEEE/ASME Trans. Mechatronics*, vol. 25, no. 6, pp. 2789–2800, Dec. 2020.
[23] L. Chen, Y. Luo, M. Bian, Z. Qin, J. Luo, and K. Li, "Estimation of tire-road friction coefficient based on frequency domain data fusion," *Mech. Syst. Signal Process.*, vol. 85, pp. 177–192, Feb. 2017.
[24] T. Chen, L. Chen, X. Xu, Y. Cai, H. Jiang, and X. Sun, "Passive fault-tolerant path following control of autonomous distributed drive electric vehicle considering steering system fault," *Mech. Syst. Signal Process.*, vol. 123, pp. 298–315, May 2019.
[25] G. Zhang, H. Zhang, X. Huang, J. Wang, H. Yu, and R. Graaf, "Active fault-tolerant control for electric vehicles with independently driven rear in-wheel motors against certain actuator faults," *IEEE Trans. Control Syst. Technol.*, vol. 24, no. 5, pp. 1557–1572, Sep. 2016.
[26] W. Li, Z. Xie, J. Zhao, and P. K. Wong, "Velocity-based robust fault tolerant automatic steering control of autonomous ground vehicles via adaptive event triggered network communication," *Mech. Syst. Signal Process.*, vol. 143, Sep. 2020, Art. no. 106798.
[27] M. B. Alberding, J. Tjønnas, and T. A. Johansen, "Integration of vehicle yaw stabilisation and rollover prevention through nonlinear hierarchical control allocation," *Vehicle Syst. Dyn.*, vol. 52, no. 12, pp. 1607–1621, Dec. 2014.
[28] J. Yoon and H. Peng, "Robust vehicle sideslip angle estimation through a disturbance rejection filter that integrates a magnetometer with GPS," *IEEE Trans. Intell. Transp. Syst.*, vol. 15, no. 1, pp. 191–204, Feb. 2014.
[29] D. Selmanaj, M. Corno, G. Panzani, and S. M. Savaresi, "Vehicle sideslip estimation: A kinematic based approach," *Control Eng. Pract.*, vol. 67, pp. 1–12, Oct. 2017.
[30] E. Hashemi, M. Pirani, A. Khajepour, A. Kasaiezadeh, S.-K. Chen, and B. Litkouhi, "Corner-based estimation of tire forces and vehicle velocities robust to road conditions," *Control Eng. Pract.*, vol. 61, pp. 28–40, Apr. 2017.
[31] E. Hashemi, M. Pirani, A. Khajepour, B. Fidan, S. Chen, and B. Litkouhi, "Fault tolerant consensus for vehicle state estimation: A cyber-physical approach," *IEEE Trans. Ind. Informat.*, vol. 15, no. 9, pp. 5129–5138, Sep. 2019.
[32] R. Skjetne and T. I. Fossen, "Nonlinear maneuvering and control of ships," in *Proc. MTS/IEEE Oceans. Ocean Odyssey. Conf.*, Nov. 2001, pp. 1808–1815.
[33] K. Kritayakirana and J. C. Gerdes, "Using the centre of percussion to design a steering controller for an autonomous race car," *Vehicle Syst. Dyn.*, vol. 50, pp. 33–51, Jan. 2012.
[34] A. Bateman, J. Hull, and Z. Lin, "A backstepping-based low-and-high gain design for marine vehicles," *Int. J. Robust Nonlinear Control*, vol. 19, no. 4, pp. 480–493, Mar. 2009.

Zhongchao Liang received the M.S. and Ph.D. degrees in mechanical engineering from the Harbin Institute of Technology, China, in 2011 and 2015, respectively.

From 2019 to 2020, he was an Academic Visitor with the Department of Electrical and Electronic Engineering, The University of Manchester, U.K. He is currently an Associate Professor with the School of Mechanical Engineering and Automation, Northeastern University, China. His research interests include intelligent vehicle and mobile robots.

Mingyu Shen received the B.S. degree in vehicle engineering from Beihua University, Jilin, China, in 2019, and the M.S. degree in transportation engineering from Northeast Forestry University, Harbin, China, in 2022. He is currently pursuing the Ph.D. degree with the School of Mechanical Engineering and Automation, Northeastern University, Shenyang, China.

His research interests include nonlinear control for intelligent vehicles and mobile robots.

Jing Zhao received the Ph.D. degree in electromechanical engineering from the University of Macau.

He is currently with the School of Mechanical Engineering and Automation, Northeastern University, China. His research interests include vehicle dynamics and control, mechanism and machine theory, fluid mechanics, and finite element analysis.

Zhongguo Li (Member, IEEE) received the B.Eng. and Ph.D. degrees in electrical and electronic engineering from The University of Manchester, Manchester, U.K., in 2017 and 2021, respectively.

He was a Research Associate with the Department of Aeronautical and Automotive Engineering, Loughborough University, Loughborough, U.K. He is currently a Lecturer in robotics and AI with the Department of Computer Science, University College London, London, U.K. His research interests include optimization and decision-making for advanced control, game theory and learning in multi-agent systems, and their applications in autonomous vehicles.

Yongfu Wang received the Ph.D. degree in control science and engineering from Northeastern University, China, in 2005.

He is currently a Professor with the School of Mechanical Engineering and Automation, Northeastern University. His research interests include fuzzy control, electric vehicle, and mechatronic systems.

Zhengtao Ding (Senior Member, IEEE) received the B.Eng. degree from Tsinghua University, Beijing, China, and the M.Sc. degree in systems and control and the Ph.D. degree in control systems from The University of Manchester Institute of Science and Technology, Manchester, U.K.

After working in Singapore for ten years, he joined The University of Manchester in 2003, where he is currently a Professor in control systems and the Head of the Control, Robotics and Communication Division. He has authored/coauthored three books, including the book *Nonlinear and Adaptive Control Systems* (IET, 2013) and has published over 300 research articles. His research interests include nonlinear and adaptive control theory and their applications, more recently network-based control, distributed optimization and distributed learning, with applications to power systems and robotics. He is a member of IEEE Technical Committee on Nonlinear Systems and Control, IEEE Technical Committee on Intelligent Control, and IFAC Technical Committee on Adaptive and Learning Systems. He is a fellow of The Alan Turing Institute and the U.K.'s National Institute for Data Science and Artificial Intelligence. He serves/has served as the Editor-in-Chief for *Drones and Autonomous Vehicles*, the Subject Chief Editor for *Nonlinear Control for Frontiers*, and an Associate Editor for *Scientific Reports*, IEEE TRANSACTIONS ON AUTOMATIC CONTROL, IEEE TRANSACTIONS ON CIRCUIT AND SYSTEMS—II: EXPRESS BRIEFS, IEEE CONTROL SYSTEMS LETTERS, *Transactions of the Institute of Measurement and Control*, *Control Theory and Technology*, *Unmanned Systems*, and several other journals.